19th Brazilian Congress of Thermal Sciences and Engineering
November 6th–10th, 2022, Bento Gonçalves - RS - Brazil

ENC-2022-0065
COMPARATIVE ANALYSIS OF STEADY-STATE GENERATION METHODS APPLIED TO THE FLOW OVER A BACKWARDS-FACING STEP

Juan Carlos Assis Silva
Leonardo Santos de Brito Alves
Programa de Pós-Graduação em Engenharia Mecânica, Universidade Federal Fluminense, Rua Passo da Pátria 156, Bloco E, Sala 211, Niterói, RJ 24210-240, Brasil
jcasilva@id.uff.br, leonardo.alves@mec.uff.br

Rômulo Bessi Freitas
Centro Federal de Educação Tecnológica Celso Suckow da Fonseca, Estrada de Adrianópolis, 1.317, Santa Rita, Nova Iguaçu, RJ 26041-271, Brasil
romulo.freitas@cefet-rj.br

Farney Coutinho Moreira
Associação Educacional Dom Bosco, Faculdade de Engenharia de Resende, Avenida Professor Antonio Esteves, 01, Campo de Aviação, Resende, RJ 27523000, Brasil
farney.coutinho@gmail.com

Abstract. *The laminar-turbulent transition over a flat plat is an important aerodynamics engineering problem. Transition delay can significantly reduce the viscous drag, since the laminar boundary layer has a lower skin friction than both transitional and turbulent ones. This is relevant as it leads to fuel use reduction. However, aerodynamic surfaces are usually not perfectly flat, due to the presence of things such as steps, junction gaps, contamination from dirt particles, and so on. Hence, it is often important to know how these roughness elements affect boundary layer transition. In order to do so, linear stability analysis is often used. One must first, however, obtain an accurate steady-state, so the governing equations of motion can be linearized around it to provide the linear disturbance equations. This can be a quite complicated task when the spatial discretization of the non-linear advection term requires specific techniques to reduce numerical oscillations due to strong gradients or discontinuities. The same is true when the flow is physically unstable, since the time integration also requires special techniques to numerically stabilize the physically unstable modes. The present work compares implicit multi-step schemes to obtain steady-states for the flow over a backward-facing step (BFS), namely the implicit Euler scheme and multi-step MGM schemes. Spatial discretization is done using a fifth-order weighted essentially non-oscillatory scheme for the inviscid fluxes and a fourth-order central-difference scheme for the viscous fluxes. This comparative analysis is performed using CPU time required to reach the imposed residue tolerances for each scheme.*

Keywords: *Backward-facing step, Steady-State, Direct Numerical Simulation.*

1. INTRODUCTION

The reduction of fuel use is a significant discussion in aviation, since may reduce the environmental impact and the operation cost. In 2006, the CO_2 emissions attributed to aviation represent just 2.5% of the total annual emissions, however, it is estimated that the high altitude emissions can be two times worse to environmental changes, when compared with the emissions on ground-level (Brueckner and Abreu, 2017; Lee *et al.*, 2004).

It is known that the laminar-turbulent transition of the flow over surfaces increase the drag force, since the laminar boundary-layer has a lower skin friction then transitional and turbulent ones, contributing to elevate the fuel consumption and also the CO_2 emissions. The prediction of the transition to turbulent of the boundary-layer flow is an important step to employ laminar flow control techniques, but the nonuniformities present in the surfaces can affect the boundary-layer transition (Hildebrand *et al.*, 2020).

Those nonuniformities, as surface gaps, steps, junction, also as dirt particles or insects present in the fluid, introduce perturbations that may be amplified in the flow by instability mechanisms, and lead to a transition to turbulence. To predict the behavior of small disturbances introduced in the laminar flow, the Linear Stability Analysis (LSA) may be employed (Schmid *et al.*, 2002; Drazin and Reid, 2004; Criminale *et al.*, 2018). Over the years, the prediction of the laminar-turbulent transition of a boundary-layer flow was carried-out using the linear stability theory, the mechanism of transition, namely Tollmien-Schlichting waves, were discoveries in the beginning of the twenty century (Tollmien, 1930; Schlichting, 1933), and in the second half of it century, numerical studies identified the unstable frequencies associated with the Blasius similarity solution of the boundary-layer equation (Mack, 1976).

As discussed above, the presence of this surfaces steps modify the boundary-layer transition, due to it, in the last years, numerous numerical (Ragab and Nayfeh, 1990) and experimental (Wang and Gaster, 2005) studies investigated the effect of surfaces steps on boundary-layer transition. Hildebrand *et al.* (2020) present a linear stability of the flow over a BFS, their results shows that the logarithmic amplification ratio is proportional to the step height, and inversely proportional to the boundary-layer thickness. In addition, their results also show that the recirculation and the reverse flow are insensitive to the BFS slope. Three-dimensional effects on transition of BFS flow were also investigated(Barkley *et al.*, 2002; Eppink *et al.*, 2018).

To employ a LSA, one must first obtain an accurate steady-state, then the original governing non-linear equation of fluid motion are linearized around it, and the perturbation (linear) equations are obtained. Obtaining accurate steady-states can be a quite complicated task, due the non-linear term in the transport equation, shock waves may be occurs. In addition, if the flow is physically unstable, the time integration scheme can be not converge to an steady-state.

If the flow is physically unstable, and the physical mode is an unstable region of the time-integration method, it will be unstable, and the steady-state do not will reached. Using implicit time-integration schemes, the numerical gain is inversely proportional to time-step (Δt), then increasing Δt is possible move the numerical mode to stable region of the method. However, as show by Santos *et al.* (2019), non-linear effects limits the maximum time-step.

The present work compares implicit multi-step schemes to obtain steady-states for the flow over a backward-facing step (BFS), namely the implicit Euler scheme and multi-step MGM schemes, presented by Teixeira and Alves (2017). This comparative analysis is performed using the number of interactions required to reach the imposed residue tolerances for each scheme.

2. Methodology

2.1 Minimal Gain Marching Scheme

Consider the non-linear dynamical system written in compact form as

$$\frac{\partial \mathbf{q}}{\partial t} = f(\mathbf{q}) \tag{1}$$

where $\mathbf{q}$ is the dependent variable vector, and $f(\mathbf{q})$ is the residue. A solution $\mathbf{q_s}$ that respects $f(\mathbf{q_s}) = 0$ is called steady-state. To time-integrate this dynamical system, Teixeira and Alves (2017) use the multi-step MGM method

$$\theta_1 \frac{\mathbf{q}^{n+1} - \mathbf{q}^n}{\Delta t} + (1-\theta_1) \frac{\mathbf{q}^{n+1} - \mathbf{q}^{n-1}}{2\,\Delta t} = \theta_2\, f^{n+1} + (1-\theta_2)\, f^n \quad , \tag{2}$$

where θ_1 and θ_2 are the control parameters. Clearly, it is possible obtain the explicit ($\theta_1 = 1$ and $\theta_2 = 0$) and implicit ($\theta_1 = 1$ and $\theta_2 = 1$) Euler methods with specific combination of the control parameters. To improve the numeric stability it is imposed restrictions $\theta_1 = 1$ and $\theta_2 \geq 1$ as demonstrated in Figure 1, where is shown the absolute value of the linear gain ($G = \mathbf{q^{n+1}}/\mathbf{q^n}$) given by employ the equation (2) to a linear problem $f(\mathbf{q}) = \lambda \mathbf{q}$.

The scheme will be numerically stable if $|G| \leq 1$, in other words, numerical errors do not will be amplified. Since the eigenvalue λ controls the system stability, i.e. the system is physically stable if $\lambda < 0$ and unstable if $\lambda > 0$ (a marginal stability scenarios occurs if $\lambda = 0$), it is easy to see that if the system is physically stable, the numerical implicit schemes will be equally stable. The same is not true, however, if the system is physically unstable. In this case, may be necessary increase the time-step in order to obtain a stable scheme when using implicit schemes.

This increasing in the time-step is limited by non-linear restrictions as show by Santos and Alves (2019) and in Santos *et al.* (2019). This is the key point on the use of multi-step MGM scheme, since the control parameters allows one to obtain a stable scheme, without increasing the time-step.

2.2 Navier-Stokes Equations

For an ideal gas, the compressible Navier-Stokes equation in conservative form and generalized coordinates are given by

$$f(\mathbf{q}) = \frac{\partial \mathcal{E}}{\partial x} + \frac{\partial \mathcal{F}}{\partial y} \tag{3}$$

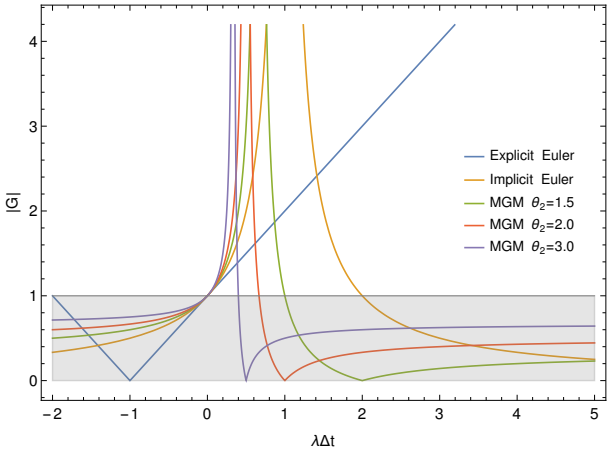

Figure 1. Linear Gain of Multi-Step MGM with $\theta_1 = 1$. Explicit Euler ($\theta_2 = 0$) and implicit Euler ($\theta_2 = 1$).

where the fluxes are defined as

$$\mathcal{E} = e_v - e_i \quad , \quad e_i = \frac{1}{J}\left(\frac{\partial \xi}{\partial x} E_i + \frac{\partial \xi}{\partial y} F_i\right) \quad , \quad e_v = \frac{1}{J}\left(\frac{\partial \xi}{\partial x} E_v + \frac{\partial \xi}{\partial y} F_v\right) \quad , \tag{4}$$

$$\mathcal{F} = f_v - f_i \quad , \quad f_i = \frac{1}{J}\left(\frac{\partial \eta}{\partial x} E_i + \frac{\partial \eta}{\partial y} F_i\right) \quad , \quad f_v = \frac{1}{J}\left(\frac{\partial \eta}{\partial x} E_v + \frac{\partial \eta}{\partial y} F_v\right) \quad , \tag{5}$$

with $q = \frac{1}{J} Q$. In the last equation, ξ and η are the metrics, and J is the determinant of jacobian matrix , the subscripts i and v means inviscid and viscous, respectively. The inviscid and viscous fluxes are given by

$$Q = \begin{bmatrix} \rho \\ \rho\, u \\ \rho\, v \\ \rho\, E \end{bmatrix} \quad , \quad E_i = \begin{bmatrix} \rho\, u \\ \rho\, u^2 + p \\ \rho\, u\, v \\ (\rho\, E + p)\, u \end{bmatrix} \quad , \quad F_i = \begin{bmatrix} \rho\, v \\ \rho\, u\, v \\ \rho\, v^2 + p \\ (\rho\, E + p)\, v \end{bmatrix} \quad , \tag{6}$$

$$E_v = \begin{bmatrix} 0 \\ \tau_{xx} \\ \tau_{xy} \\ u\,\tau_{xx} + v\,\tau_{xy} - \dot{q}_x \end{bmatrix} \quad , \quad F_v = \begin{bmatrix} 0 \\ \tau_{yx} \\ \tau_{yy} \\ u\,\tau_{yx} + v\,\tau_{yy} - \dot{q}_y \end{bmatrix} \quad . \tag{7}$$

Finally, the shear stress components, and the heat transfer flux are defined as

$$\tau_{xx} = 2\mu \frac{\partial u}{\partial x} + \lambda \left(\frac{\partial u}{\partial x} + \frac{\partial v}{\partial y}\right) \quad , \tag{8}$$

$$\tau_{yy} = 2\mu \frac{\partial v}{\partial y} + \lambda \left(\frac{\partial u}{\partial x} + \frac{\partial v}{\partial y}\right) \quad , \tag{9}$$

$$\tau_{xy} = \tau_{yx} = \mu \left(\frac{\partial u}{\partial x} + \frac{\partial v}{\partial y}\right) \quad , \tag{10}$$

$$\dot{q}_x = -k \frac{\partial T}{\partial x} \quad \text{and} \tag{11}$$

$$\dot{q}_y = -k \frac{\partial T}{\partial y} \quad . \tag{12}$$

Here, k is the thermal conductivity of the fluid, μ is the dynamic viscosity, λ is the second viscosity coefficient, where the stokes assumption is imposed ($\lambda = -\frac{2}{3}\,\mu$). Since the system of equations have five dependent variables, and just four equations, the ideal gas law, is employed

$$p = \rho\, R\, T \quad . \tag{13}$$

The dimensionless form of the governing equation are obtained using references quantities, in order to express dimensionless variables. In this work, the reference velocity is the speed of sound in the medium. In this way, the dimensionless variables are giver by

$$\rho^* = \frac{\rho}{\rho_\infty}, \quad u^* = \frac{u}{a_\infty}, \quad v^* = \frac{v}{a_\infty}, \quad x^* = \frac{x}{L_R}, \quad y^* = \frac{y}{L_R}, \quad p^* = \frac{p}{\rho_\infty\, a_\infty^2}, \quad T^* = \frac{T}{T_\infty}, \quad t^* = \frac{t}{L_R/a_\infty}, \tag{14}$$

where a_∞ is the speed of sound in the medium, L_R is the reference length scale, the subscript ∞ represent the free stream values and the superscript $*$ represent the dimensionless variables.

2.3 Mesh and Geometry

Initially a single block, without corners and discontinuities, structured grid is construct with a continuous slop given by the function

$$y_w = \begin{cases} 0, & \text{if } x < x_s \\ -\frac{h}{2}\left(1 + cos\left[\pi\left(\frac{x-x_s}{x_f-x_s}+1\right)\right]\right), & \text{if } x_s \leq x \leq x_f \\ -h, & \text{if } x > x_f \end{cases} \tag{15}$$

where x_s and $x_f = x_s + h/tan(\theta)$ represent the beginning and the end points of the step, h is the step height and θ is the maximum slop of BFS. This geometry matches with the one presented by Hildebrand *et al.* (2020). As it is a $\mathcal{C}^1$ shape (the second derivative has a discontinuity), that is not the best geometry to apply a finite difference scheme, since this discontinuities may be insert local errors. The parameters used to construct the mesh used in the present work are displayed in Table 1.

x_s	θ	h
1.0	40°	1.0

Table 1. Mesh geometry parameters.

The mesh was build using a elliptic grid generation method (Thompson, 1982), and a orthogonality boundary condition is imposed on the step wall. The Figure 2 shows an close-up of the grid near the step. After some explicit simulation, was noted that the piecewise shape introduce numerical errors, this error induce a time-step restriction to the implicit time-marching schemes. In order to eliminate this effect, a $\mathcal{C}^\infty$ shape was developed and is presented in Equation (16).

$$y_w = -\frac{1}{2}\left[1 + Tanh[3(x-1.6)]\right] \tag{16}$$

Figure 2 (Right) show a comparison between the initial and final shapes for the slope.

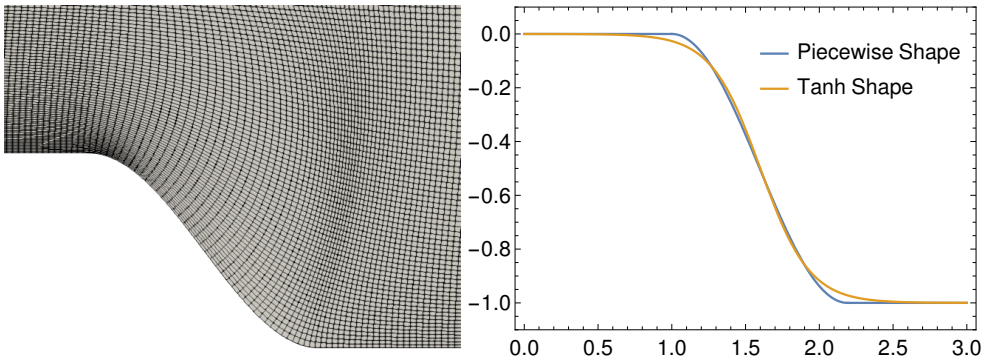

Figure 2. Close-up on the Backward-Facing Step (Left), Piecewiese and $\mathcal{C}^\infty$ slope shapes (right)

2.4 Numerics

To perform the numerical simulation the 3D4S (Three-Dimensional Structured Steady-State Solver) by Santos (2020) was used. The code is higly accurate to obtain both steady and unsteady solutions, it has several time-marching as well as conservative high order spatial discretizations schemes and was built using the PETSc library (Abhyankar *et al.*, 2018) that supports the scalable (parallel) solution.

In the present work, A fifth order WENO type scheme (Jiang and Shu, 1996) for inviscid fluxes, combined with a centered fourth order conservative scheme for the diffusive fluxes are applied. Different multi-step MGM control parameters were applied to time-marching.

The velocity field is prescribed at the inlet, and extrapolated at the outlet. No slip condition, and zero gradient for both, pressure and temperature (adiabatic wall), are imposed at the wall. Free-stream conditions are imposed on the far-field, except the v component of velocity where a zero gradient condition was imposed. In order to allow a well-posed problem, the inlet velocity profile was taken at $x = 0.2$ from the leading-edge of a Finite Volume Solution given by LeMANS code Moreira *et al.* (2021). The simulation dimensionless parameters are $Ma = 0.5$, $Re = 200$, $Pr = 0.72$, and the characteristic length is the step height.

3. RESULTS

Initially a mesh convergence study was carried out using different grids and comparing the residue and the profile of primitive proprieties. This results are present in Figure 3 and show good agreement for all grids used. Although show near equal results, the grid with less points, reached to steady-state with worse machine precision then others gris.

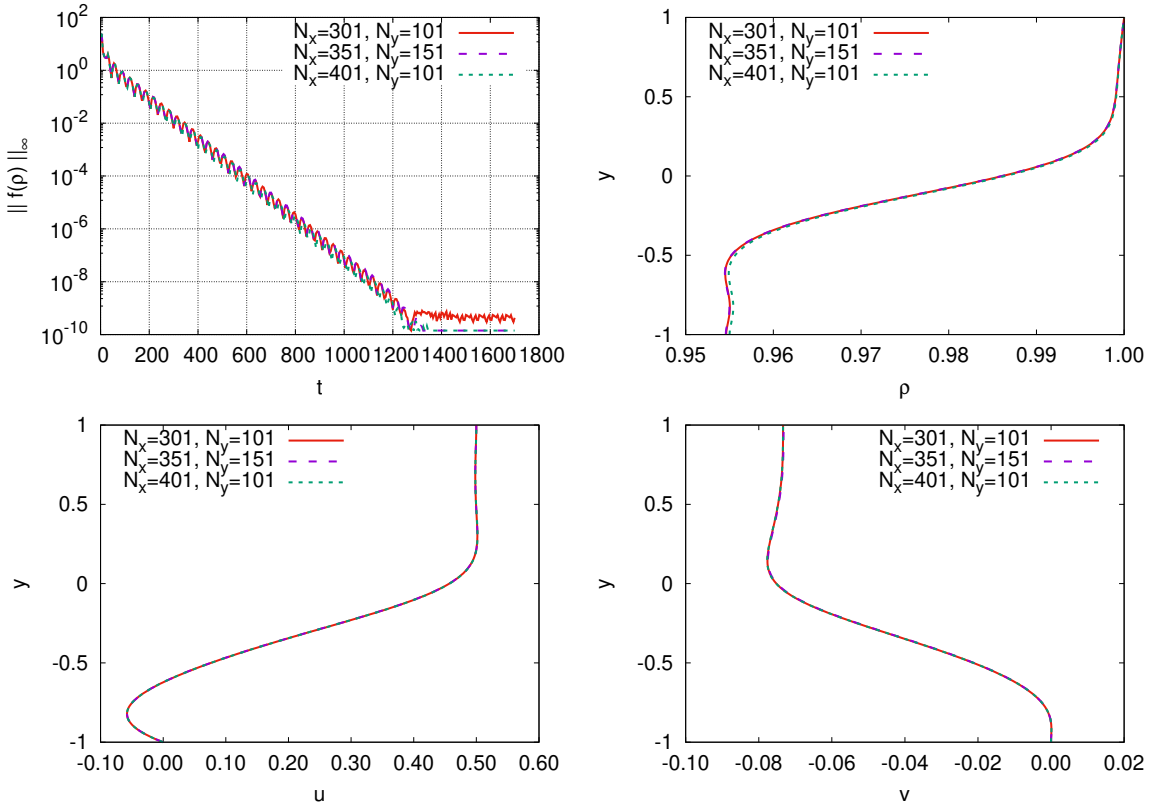

Figure 3. Comparison between steady-states obtained with different grids. L_∞ norm of $f(\rho)$ versus simulation time (Upper Lefet), vertical profile at $x = 3.0$ for fluid density (Upper Right), horizontal velocity (Bottom Left) and vertical velocity (Bottom Right).

In order to verify the results obtained in this work, and provide inlet conditions, the steady-steady was compared with a solution obtained with finite volume LeMANS code by Moreira *et al.* (2021). The comparison was done for the Mach number profile for a given horizontal position ($x = 2.3$) and can be seen in Figure 4 (Left). In addition, Figure 4 (Right) shows the Mach number field, also for both codes.

Since the LeMANS results are reached using second order spatial discretization scheme, a considerable numerical diffusion is observed in the LeMANS results, when compared with 3D4S ones, that can be reduced through grid refinement. Although, the Mach number vertical profile obtained with both codes are very similar and inside of the recirculation bubble the results are nearly equal.

Figure 5 shows all the flow fields, top-down fluid density, horizontal velocity (positive sign is to right), vertical velocity (positive sign is to upper), pressure, temperature, and Mach number. It is important to note that all flow fields behavior are very similar with results presented by Hildebrand *et al.* (2020) in a comparative sence. The horizontal velocity profile shows a recirculation zone soon after step, that is induced by the adverse pressure gradient. It means that after the step, the pressure increase in the flow direction, then the fluid is decelerate until return in the step direction.

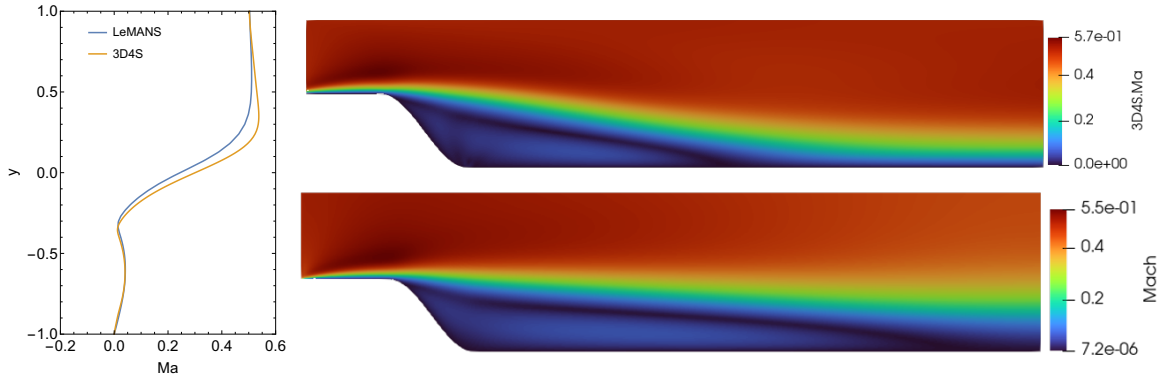

Figure 4. Comparison between Mach number vertical profile at $x = 2.3$, for LeMANS and 3D4S codes (Left) and Mach number fields for 3D4S (upper right) and LeMANS (bottom right).

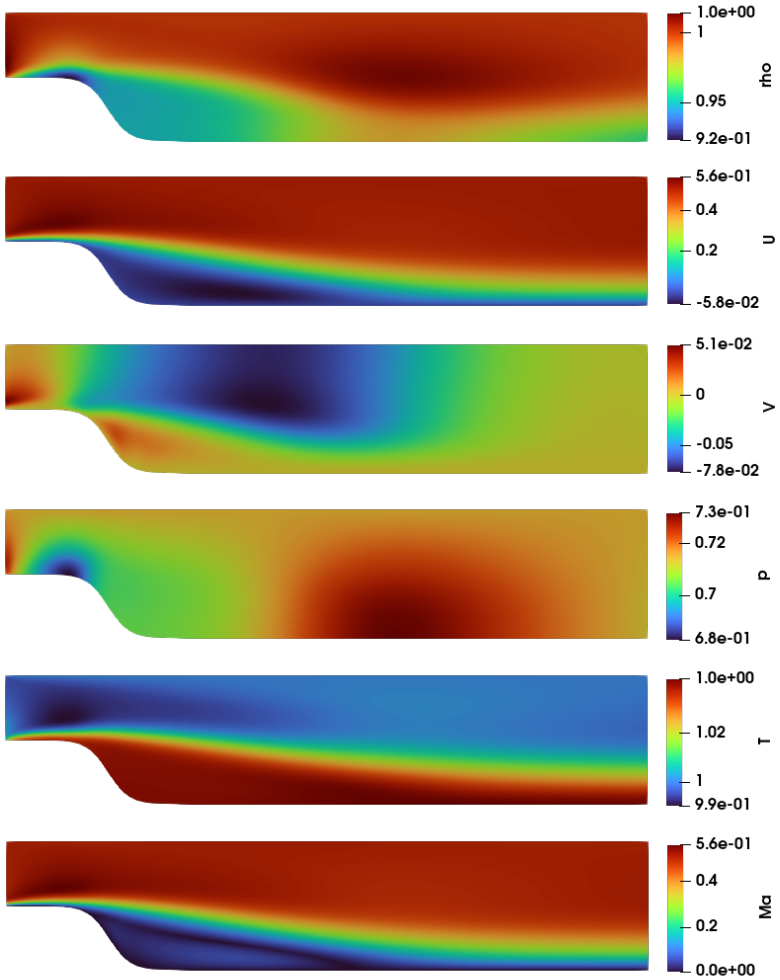

Figure 5. Flow fields steady-state obtained with 3D4S. In top-down order fluid density, horizontal velocity (positive sign is to right), vertical velocity (positive sign is to upper), pressure, temperature, and Mach number.

In vertical velocity field, the region before the step has a classical boundary-layer behavior, the fluid need go up to conserve mass, since the horizontal velocity is reduced by skin friction. Although, in the region closer to the step, a suction effect is observed, then the fluid is forced go down, and fluid come in by upper boundary. Inside of recirculation zone, the fluid go up again, since the low pressure point is located at slope beginning.

Finally the comparative analysis is show in Figure 6. The CPU time required to reach the convergence criterion $||f(\mathbf{q})||_\infty \leq 10^{-6}$ is plotted versus the time-step used. As well as previously discussed, the non-linear maximum time-step restriction prohibit increase the time-step overly, however, the maximum time-step is correlated with the time-

marching scheme. Hence, the maximum time-step observed for implicit Euler scheme $\left(0.7 \times 10^{-3}\right)$ was greater then the observed for Multi-Step MGM scheme $\left(0.4 \times 10^{-3}\right)$.

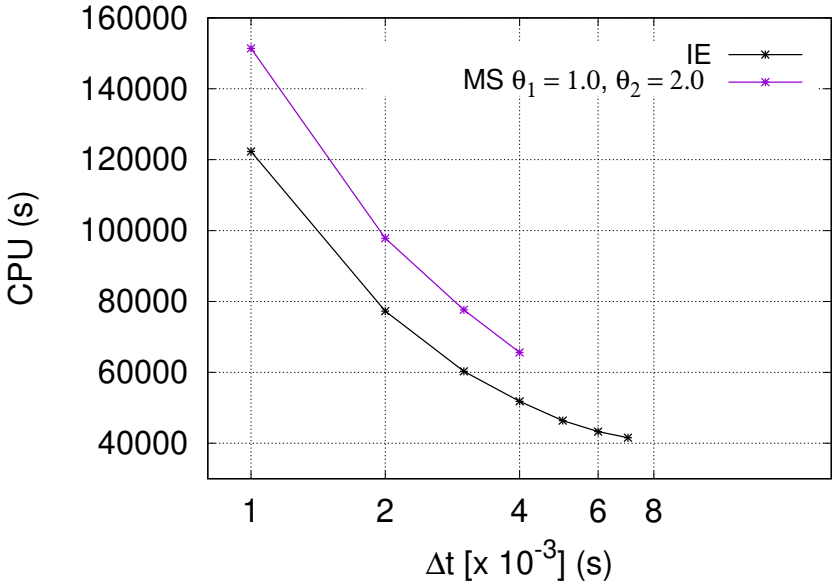

Figure 6. CPU time used to reach $||f(\mathbf{q})||_\infty \leq 10^{-6}$ *versus* time-step used in each simulation. The red line are the data for Implicit Euler scheme ($\theta_1 = 1$ and $\theta_2 = 1$) when the yellow line are the data for Multi-Step MGM with $\theta_1 = 1$ and $\theta_2 = 2$.

Since this flow is physically stable, MS-MGM linear gain is greater then Implicit Euler, as show Figure 1. Hence, was expected that the CPU time needed with the former would be also greater then the latter. That is exactly what Figure 6 shows, it means that more time is need to reach the same convergence using Multi-step MGM instead of implicit Euler scheme when the flow is physically stable.

4. CONCLUSIONS

In this work, two different implicit time-marching scheme were applied to Navier-Stokes equations in order to obtain an accurate steady-state of the flow over a backwards-facing step. Initially, the results were validated through comparison with a finite volume solution with same conditions.

Despite the good agreement of velocity profile inside of recirculation bubble obtained with both codes, the finite volume solution contains excessive numerical diffusion, which can be easily observed in the length of the bubble. It is one of the attributes of the higher-order method, no excessive numerical diffusion is needed to guarantee a real time-independent steady-state. Even with relatively few refined grids, the use of high order discretization schemes allows to obtain mesh convergence, and accurate steady-state, as shown in Figure 3.

The comparative performance analysis between MS-MGM and implicit Euler schemes were presented, and the results show that the former is more efficient the latter in this test case. It is important to emphasize that the flow stability is a crucial point here, since the flow is stable, the MS-MGM linear gain is greater than implicit Euler, that is not true if the flow be physically unstable for certain time-steps.

Natural future work is to apply the multi-stage MGM at the same problem, and compare with both methods discussed in this work. After that, a physically unstable test case must be used to understand the behavior of those method in that scenarios.

5. ACKNOWLEDGMENTS

JCAS gratefully acknowledgment support of CAPES for graduate scholarship. The authors would like to thank the support received from AFOSR (SOARD) Grant FA9550-18-1-0419 with Dr. Sarah Popkin as Program Officer. Any opinions, findings, and conclusions or recommendations expressed in this material are those of the authors and do not necessarily reflect the views of the United States Air Force Office of Scientific Research or the United States Government.

The authors acknowledge the National Laboratory for Scientific Computing (LNCC/MCTI, Brazil) for providing HPC resources of the SDumont supercomputer, which have contributed to the research results reported within this paper. URL: http://sdumont.lncc.br.

6. REFERENCES

Abhyankar, S., Brown, J., Constantinescu, E.M., Ghosh, D., Smith, B.F. and Zhang, H., 2018. "Petsc/ts: A modern scalable ode/dae solver library". *arXiv preprint arXiv:1806.01437*.

Barkley, D., Gomes, M.G.M. and Henderson, R.D., 2002. "Three-dimensional instability in flow over a backward-facing step". *Journal of fluid mechanics*, Vol. 473, pp. 167–190.

Brueckner, J.K. and Abreu, C., 2017. "Airline fuel usage and carbon emissions: Determining factors". *Journal of Air Transport Management*, Vol. 62, pp. 10–17. ISSN 0969-6997. doi:https://doi.org/10.1016/j.jairtraman.2017.01.004. URL `https://www.sciencedirect.com/science/article/pii/S0969699716302976`.

Criminale, W.O., Jackson, T.L. and Joslin, R.D., 2018. *Theory and computation in hydrodynamic stability*. Cambridge University Press.

Drazin, P.G. and Reid, W.H., 2004. *Hydrodynamic stability*. Cambridge university press.

Eppink, J.L., Wlezien, R.W., King, R.A. and Choudhari, M., 2018. "Interaction of a backward-facing step and crossflow instabilities in boundary-layer transition". *AIAA Journal*, Vol. 56, No. 2, pp. 497–509.

Hildebrand, N., Choudhari, M.M. and Paredes, P., 2020. "Predicting boundary-layer transition over backward-facing steps via linear stability analysis". *AIAA Journal*, Vol. 58, No. 9, pp. 3728–3734.

Jiang, G.S. and Shu, C.W., 1996. "Efficient implementation of weighted eno schemes". *Journal of computational physics*, Vol. 126, No. 1, pp. 202–228.

Lee, J.J., Lukachko, S.P. and Waitz, I.A., 2004. "Aircraft and energy use".

Mack, L.M., 1976. "A numerical study of the temporal eigenvalue spectrum of the blasius boundary layer". *Journal of Fluid Mechanics*, Vol. 73, No. 3, pp. 497–520.

Moreira, F.C., Wolf, W.R. and Azevedo, J.L.F., 2021. "Thermal analysis of hypersonic flows of carbon dioxide and air in thermodynamic non-equilibrium". *International Journal of Heat and Mass Transfer*, Vol. 165, p. 120670. ISSN 0017-9310. doi:https://doi.org/10.1016/j.ijheatmasstransfer.2020.120670. URL `https://www.sciencedirect.com/science/article/pii/S0017931020336061`.

Ragab, S. and Nayfeh, A., 1990. "Stability of compressible boundary layers over a smooth backward-facing step". In *21st Fluid Dynamics, Plasma Dynamics and Lasers Conference*. p. 1449.

Santos, R.D. and Alves, L.S., 2019. "Generation of steady-states with discontinuities using minimal gain marching schemes". In *AIAA Aviation 2019 Forum*. p. 2839.

Santos, R.D., Volpini, M.R. and Alves, L.S., 2019. "Nonlinear time-step restriction on minimal gain marching schemes". In *COBEM-2019*.

Santos, R.D.d., 2020. *Um estudo sobre os métodos de Runge-Kutta com forte estabilidade linear e não linear*. Ph.D. thesis, Universidade Federal Fluminense.

Schlichting, H., 1933. "Zur enstehung der turbulenz bei der plattenströmung". *Nachrichten von der Gesellschaft der Wissenschaften zu Göttingen, Mathematisch-Physikalische Klasse*, Vol. 1933, pp. 181–208.

Schmid, P.J., Henningson, D.S. and Jankowski, D., 2002. *Stability and transition in shear flows.*, Vol. 55. Springer.

Teixeira, R. and Alves, L., 2017. "Minimal gain marching schemes: searching for unstable steady-states with unsteady solvers". *Theoretical and Computational Fluid Dynamics*, Vol. 31, No. 5, pp. 607–621.

Thompson, J.F., 1982. "Elliptic grid generation". *Applied Mathematics and Computation*, Vol. 10-11, pp. 79–105. ISSN 0096-3003. doi:https://doi.org/10.1016/0096-3003(82)90188-6. URL `https://www.sciencedirect.com/science/article/pii/0096300382901886`.

Tollmien, W., 1930. "Über die entstehung der turbulenz". In *Vorträge aus dem Gebiete der Aerodynamik und verwandter Gebiete*, Springer, pp. 18–21.

Wang, Y. and Gaster, M., 2005. "Effect of surface steps on boundary layer transition". *Experiments in Fluids*, Vol. 39, No. 4, pp. 679–686.

7. RESPONSIBILITY NOTICE

The authors are the only responsible for the printed material included in this paper.